Thin-Walled Structures 188 (2023) 110879

Contents lists available at ScienceDirect

Thin-Walled Structures

journal homepage: www.elsevier.com/locate/tws

Temperature effect on buckling behavior of prestressed CFRP-reinforced steel columns

Lili Hu [a,b], Xu Liang [a,b], Peng Feng [c], Hai-Ting Li [a,b,*]

[a] State Key Laboratory of Ocean Engineering, School of Naval Architecture, Ocean and Civil Engineering, Shanghai Jiao Tong University, Shanghai, 200240, China
[b] Shanghai Key Laboratory for Digital Maintenance of Buildings and Infrastructures, Shanghai Jiao Tong University, Shanghai 200240, China
[c] Key Laboratory of Civil Engineering Safety and Durability of China Education Ministry, Department of Civil Engineering, Tsinghua University, Beijing 100084, China

ARTICLE INFO

Keywords:
Temperature effect
Extreme temperature
Composite structure
FRP
Steel column

ABSTRACT

Prestressed carbon fiber reinforced polymer (CFRP)-reinforced steel columns behave differently under extreme temperature conditions because CFRP prestress changes with temperatures varying and is a key factor influencing the buckling behavior of such columns. This paper deeply studies the temperature effect on the buckling behavior of the composite columns. First, varying material properties from −80 to 80 °C are studied, and the temperature effect mechanism on the buckling behavior of such column is investigated. Moreover, analyses of two temperature situations are conducted using finite element modeling. When the column is loaded at a certain temperature, the buckling capacity maintains almost constant with temperature varying from 20 to 80 °C, while it increases 3%–7% when the temperature drops from 20 to −80 °C. When the column is preloaded and then the temperature changes, from 20 to 80 °C, the column extends, and the deformation is first symmetric and global and then changes to local and asymmetric when the temperature reaches a turning point; from 20 to −80 °C, the column shrinks, and the deformation is symmetric and global. Additionally, varying temperature may lead to a large change in CFRP stress (as high as 321.9 MPa), which causes significant reduction in the buckling capacity (as much as 18%). These findings provide valuable references for the design of such columns and related thin-walled structures under extreme temperature conditions.

1. Introduction

Extreme temperatures occurred in the world. The coldest temperature was −89.2 °C [1,2]; the highest air temperature was above 53 °C, and the ground temperatures are considerably higher [3]. Notably, in the summer of 2022, very high temperature weather patterns occurred in the U.S., China, Spain, India and other places [4,5]. For example, an intense heatwave swept through northern India with temperatures hitting 49.2 °C. The temperature difference between day/night or different seasons is also large, as shown in Fig. 1 [5,6]. For example, for many places in the middle of the USA, the temperature varies from −34.4 °C to 43.3 °C from winter to summer. Considering the effects of global warming and the explorations of extreme environments, such situation is likely to last for a long time and even become serious in the future [5].

Many structures are exposed to the natural environment and are therefore subjected to extreme temperatures and periodically changing atmospheric temperatures over the long term. Due to the function of solar radiation, the temperature difference of structures could be much higher than air temperature difference [7]. Composite structures composed of different materials (e.g., steel, concrete, fiber reinforced polymer (FRP)) are widely applied in civil engineering [8–10], and those materials show significant differences in thermal performance. Therefore, the temperature effect is one of the major factors dominating the designs and applications [11]. There have been many valuable studies on the temperature effect of steel-concrete composite structures [12,13]. It is found that the periodic change in temperature (i.e., annual/daily temperature cycle) and the sudden temperature change may lead to cracks and even structural damage. For example, the Foreland bridge of the River Main Bridge in Germany dropped by 38 cm and caused numerous cracks in its superstructure due to extremely high temperature [14].

FRP material, known for its high strength, light weight, and excellent durability, has been increasingly employed in the construction of buildings and bridges. Studies on FRP-steel composite structures show the advantages of good flexural behavior [15,16], buckling behavior [17,18] and fatigue behavior [19,20]. These structures also face a similar situation of temperature effects for the following two reasons. First, steel has a positive coefficient of thermal expansion (CTE), while

* Corresponding author at: State Key Laboratory of Ocean Engineering, School of Naval Architecture, Ocean and Civil Engineering, Shanghai Jiao Tong University, Shanghai, 200240, China.
E-mail address: haiting.li@sjtu.edu.cn (H.-T. Li).

https://doi.org/10.1016/j.tws.2023.110879
Received 16 January 2023; Received in revised form 11 April 2023; Accepted 15 May 2023
Available online 3 June 2023

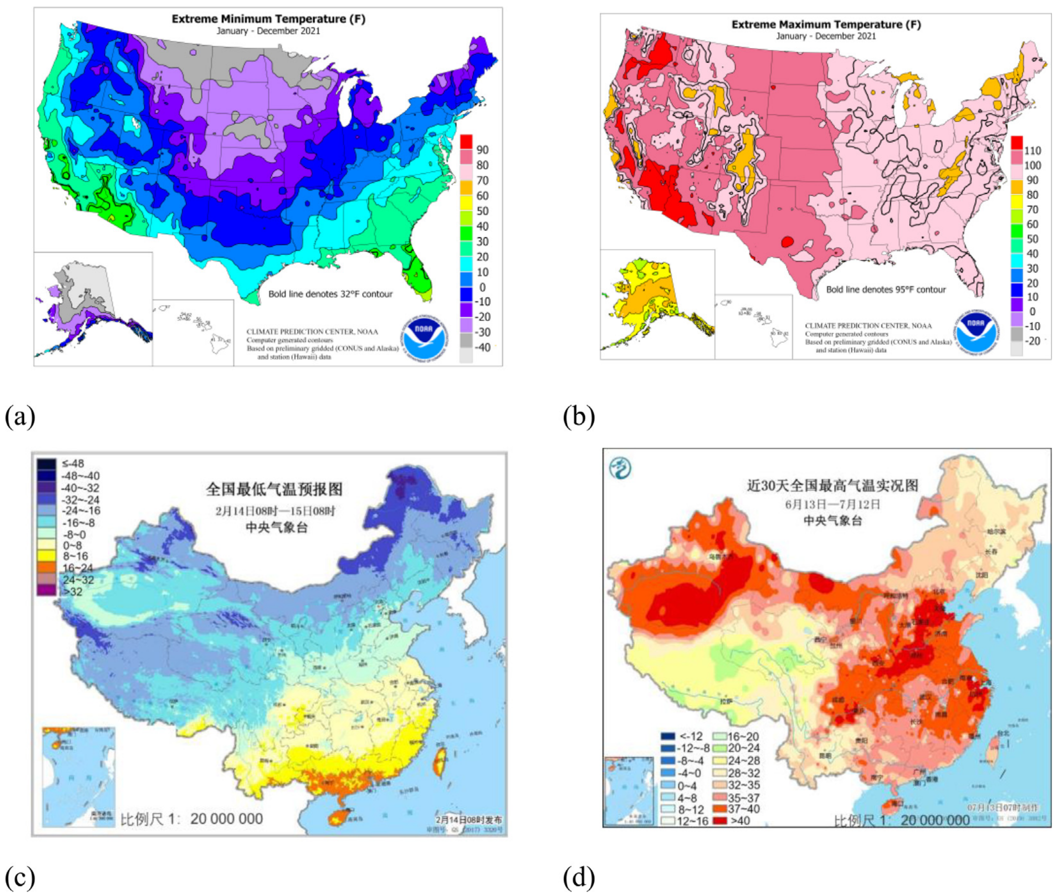

Fig. 1. Large temperature differences between seasons: (a) Minimum temperature in 2021 in the U.S., (b) Maximum temperature in 2021 in the U.S., (c) Minimum temperature in 14–15, Feb, 2021 in China, (d) Maximum temperature in June–July, 2021 in China.

the FRP's CTE is close to 0 [21]. Second, the properties of steel and FRP materials change with temperature [21–23]. Specifically, for FRP bonded steel structures, the behavior and failure mode are determined by the adhesive properties and are influenced by temperature [24–26]. For steel structures anchored with FRPs, this influence can be mitigated, but due to the mismatch of the CTE between steel and CFRP materials, the CFRP stress increases as the temperature increases [27,28], which could lead to behavior change in the structures.

Specifically, a prestressed CFRP-reinforced steel column was proposed [29], which can have a buckling capacity 1.5 times higher than that of a pure steel column under axial compression [30]. It is composed of a steel column, two prestressed CFRP laminates, two prestressing chairs, and two anchorages, as shown in Fig. 2. The high buckling capacity is attributed to the prestressed CFRPs, which restrain the lateral displacement at the midspan of the steel column and reduce the initial imperfection due to the self-balancing procedure [29,30]. This type of column is similar to prestressed stayed column [31–33], both of which are suitable for open structures, bridges, tall buildings, and towers where slender components are required. They have been successfully applied in "Rock in Rio III" stadium in Brazil and Algarve Stadium in Portugal [32,34]. Notably, the thermal stress not only affects the stress state of the steel structure but also changes the CFRP stress, which directly affects the buckling capacity and stiffness of this member due to the special self-balancing system [30,35]. Therefore, prestressed CFRP-reinforced steel columns are more sensitive to temperature, and the mechanism is more complex compared with other composite components; thus, the temperature effect of this member should be seriously considered.

Many significant research works on prestressed stayed columns have been conducted at room temperature (e.g. [31–33]), while its behavior considering temperature effect is limited. Zhou et al. [36] studied the behavior of prestressed steel stayed columns under fire and found that the failure was dependent on prestress level and external load at high temperature. Hu et al. [37] investigated the behavior of prestressed CFRP-reinforced steel column under fire and proposed a design method. These two types of columns in [36] and [37] behave differently due to the different mechanical and thermal property change of the prestressed materials (e.g. steel and FRP) with temperature. In addition, as stated above, in real engineering, even if fire does not occur, the slow temperature change could also have a large influence on this member. Considering the recorded lowest/highest temperatures and the increasingly intense greenhouse effect, the temperature range studied in this paper was selected from −80 °C to 80 °C, which could cover the possible temperature range of the structure. To the best of our knowledge, related studies on the temperature effect of this range on prestressed CFRP-reinforced steel column have not been carried out thus far, which may hinder the real applications of this member.

Therefore, this paper conducts a systematic study on the temperature effect on the buckling behavior of prestressed CFRP-reinforced steel columns based on the typical specimens in Ref. [30]. The temperature effect on the material properties and the temperature effect mechanism on the component are firstly studied. Then, the influence of temperature on the CFRP prestress (T_i) and buckling capacity (P_b) relationship is analyzed by finite element method (FEM). In addition, the situation that the column is preloaded and then the temperature changes is also considered using FEM. Large displacement and stress changes are obtained and analyzed; parameter influencing rules on the thermal sensitivity of such columns are revealed. Finally, the change in buckling capacity of the preloaded column after the temperature changes is obtained, which provides good references for the design of such columns.

Table 1
Mechanical properties of the steel at different temperatures.

θ (°C)	E_s (GPa)	$(E_s - E_{sr})/E_{sr}$	f_y (MPa)	$(f_y - f_{yr})/f_{yr}$	f_u (MPa)	$(f_u - f_{ur})/f_{ur}$
−80	223	8.3%	744	9.1%	845	10.5%
−60	219	6.3%	724	6.2%	821	7.3%
−40	215	4.4%	706	3.5%	800	4.6%
−20	211	2.4%	689	1.0%	781	2.1%
0	208	1.0%	674	−1.2%	763	−0.3%
20 to 80	206	0.0%	682	0.0%	765	0.0%

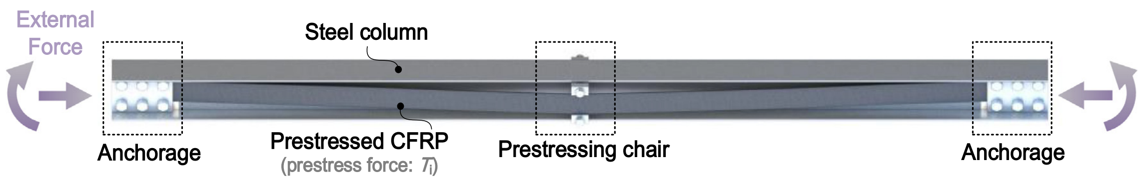

Fig. 2. Prestressed CFRP-reinforced steel column.

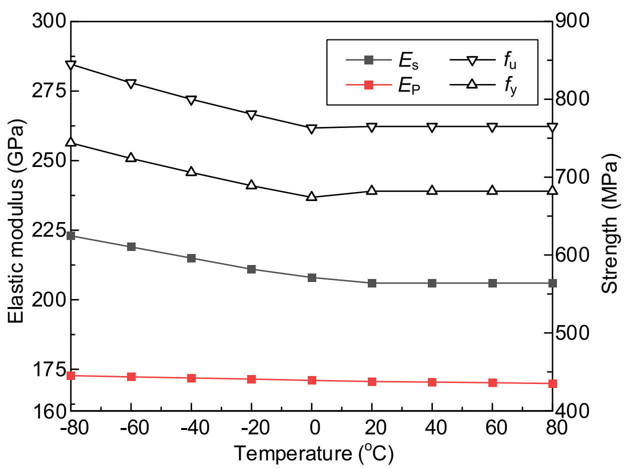

Fig. 3. Influence of temperature on the mechanical properties of steel and CFRP.

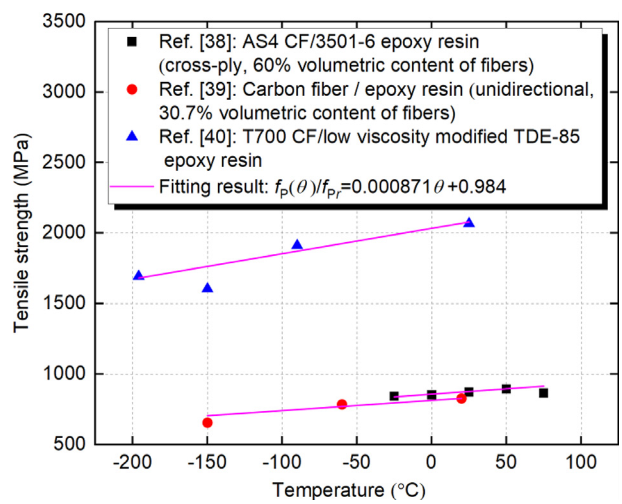

Fig. 4. Low temperature model of CFRP strength.

2. Temperature effect

2.1. Temperature effect on mechanical and thermal properties of materials

(1) Mechanical properties

For the Q690 steel, the material properties at ambient temperature are as follows: the yield point (f_y), ultimate strength (f_u) and elastic modulus (E_s) are 682 MPa, 765 MPa and 206 GPa, respectively [30]. Based on Refs. [22,23], the mechanical properties of this steel at different temperatures can be calculated, and the calculated formulas of E_s and f_y are Eqs. (1) and (2), respectively. θ (°C) is an arbitrary temperature, and the subscript r of parameters (i.e., E_{sr}, f_{yr}, f_{ur}, E_{Pr}, f_{Pr} and CTE_{sr}) refers to their values at room temperature (20 °C). Based on this, the mechanical properties of this steel at −80 to 80 °C are calculated, as shown in Table 1 and Fig. 3. An obvious improvement in material properties was found from 20 to −80 °C, while the corresponding decrease from 20 to 80 °C was very limited.

$$E_s(\theta) = \begin{cases} \dfrac{1}{1+(\theta/534)^{5.5}} E_{sr} \ (20 < \theta \le 80) \\ 3.068 E_{sr}(\theta + 273.15)^{-0.198} \ (-80 \le \theta \le 20) \end{cases} \tag{1}$$

$$f_y(\theta) = \begin{cases} \dfrac{1}{1+(\theta/538)^{10}} f_{yr} \ (20 < \theta \le 80) \\ 1.975 f_{yr}^{1.139}(\theta + 273.15)^{-0.285} \ (-80 \le \theta \le 20) \end{cases} \tag{2}$$

For the CFRP laminates at ambient temperature, the elastic modulus (E_P) and the ultimate strength (f_P) are 171 GPa and 2450 MPa, respectively. The reduction in the strength and stiffness of CFRP at high temperatures can be defined by Eqs. (3)–(4) [21]. Low temperature increases the probability of stress concentration and results in degradation of the CFRP strength. Due to the difficulty of obtaining valid data of CFRP strength at low temperatures [38], a reduction factor in CFRP strength is proposed by fitting existing experimental data [38–40] (Fig. 4), as shown in Eq. (3). E_P for unidirectional CFRP laminates depends on the carbon fibers and the matrix and is therefore affected by temperature with the same tendency as that of the matrix [41]. Because the fiber volumetric content is approximately 80% for the CFRP, E_P at low temperature can be obtained. The mechanical properties of CFRP at high/low temperatures are summarized in Table 2 and shown in Figs. 3 and 4. Because the volumetric content of fibers is very high for this CFRP, the increase in E_P under low temperature is not obvious.

$$f_P(\theta)/f_{Pr} = \begin{cases} 0.45\tanh[-5.83\times10^{-3}(\theta - 339.54)] + 0.55 \ (20 < \theta \le 80) \\ 0.000871\theta + 0.984 \ (-80 \le \theta \le 20) \end{cases} \tag{3}$$

$$E_P(\theta)/E_{Pr} = 0.475\tanh[-8.68\times10^{-3}(\theta - 367.41)] + 0.525 \ (20 < \theta \le 80) \tag{4}$$

(2) Thermal properties

The thermal properties include the unit mass ρ, the thermal conductivity λ, CTE and specific heat c. The subscripts s and P represent steel and CFRP, respectively.

Table 2
Mechanical properties of the CFRP at different temperatures.

θ (°C)	f_P (MPa)	$(f_P - f_{Pr})/f_{Pr}$	E_P (GPa)	$(E_P - E_{Pr})/E_{Pr}$
−80	2240	−8.6%	172.7	1.2%
−60	2283	−6.8%	172.3	1.0%
−40	2325	−5.1%	171.9	0.8%
−20	2368	−3.3%	171.5	0.5%
0	2411	−1.6%	171.0	0.2%
20	2450	0.0%	170.6	0.0%
40	2384	−2.7%	170.4	−0.1%
60	2368	−3.3%	170.2	−0.2%
80	2348	−4.2%	169.9	−0.4%

Table 3
The thermal properties of the steel at different temperatures.

θ (°C)	ρ_s (kg/m^3)	λ_s (W/(m K))	CTE$_s$ (10^{-6} °C^{-1})	c_s (kJ/(kg K))
−80		53.33	11.8	0.415
−60		53.33	12.3	0.426
−40		53.33	12.8	0.437
−20		53.33	13.3	0.445
0	7850	53.33	13.7	0.46
20		53.33	14.3	0.440
40		52.67	14.3	0.453
60		52.00	14.3	0.466
80		51.34	14.4	0.477

For steel, ρ_s is 7850 kg/m^3. λ_s at high temperature can be calculated by Eq. (5) [42]; λ_s slightly changes within the range of 0 to −80 °C [43], and thus, its value at low temperature is taken as the value at 20 °C (i.e., 53.33 W/(m K)). c_s at high temperature is calculated by Eq. (6) [42]; c_s at low temperature is proposed by fitting credible experimental data from the literature [44] (Fig. 5(a)), as shown in Eq. (6), which is in good accordance with [42]. The thermal strain $(\Delta l/l)_s$ can be calculated by Eq. (7) when θ ranges from 25 to 720 °C [45], which is in good accordance with [42], and CTE$_s$ equals $(\Delta l/l)_s/\Delta\theta$; CTE$_s$ at low temperature under 25 °C is proposed by fitting credible experimental data from the literature [46] (Fig. 5(b)), as shown in Eq. (7). The thermal properties of steel at high/low temperatures are summarized in Table 3.

$$\lambda_s = \begin{cases} 54 - 0.0333\theta \ \ (\mathrm{W/(m\ K)}) \ \ (20 < \theta \le 80) \\ 53.33 \ \ (\mathrm{W/(m\ K)}) \ \ (-80 \le \theta \le 20) \end{cases} \tag{5}$$

$$c_s = \begin{cases} 425 + 0.773\theta - 1.69 \times 10^{-3}\theta^2 + 2.22 \times 10^{-6}\theta^3 \ (\mathrm{J/(kg\ K)}) \ \ (20 < \theta \le 80) \\ 0.000568\theta + 0.46 \ (\mathrm{J/(kg\ K)}) \ \ (-80 \le \theta \le 20) \end{cases} \tag{6}$$

$$\begin{cases} (\Delta l/l)_s = 1.42 \times 10^{-5} \cdot \theta + 0.113 \times 10^{-8} \cdot \theta^2 - 3.545 \times 10^{-4} \ \ (25 < \theta \le 80) \\ \mathrm{CTE}_s = (0.00167\theta + 0.96) \cdot \mathrm{CTE}_{sr} \ \ (-80 \le \theta \le 25) \end{cases} \tag{7}$$

For CFRP, the unit mass ρ_P is 1600 kg/m^3. CTE$_P$ varies slightly between −80 °C and 20 °C [47] and thus is taken as the value at ambient temperature (0 °C^{-1}) [21] for the temperature range studied in this paper. λ_P at high temperature is calculated by Eq. (8) [21]; λ_P varies slightly between −80 °C and 0 °C [48], and thus, λ_P at low temperature is set the same as that at 0 °C (i.e., 1.4 W/(m °C)). c_P at high temperature is calculated by Eq. (9) [21]; c_P at low temperature is assumed to be the same as that at 0 °C due to limited studies. The thermal properties of CFRP at high/low temperatures are summarized in Table 4.

$$\lambda_P = \begin{cases} 1.4 + \dfrac{-1.1}{500}\theta \ (\mathrm{W/(m\ °C)}) \ (0 < \theta \le 80) \\ 1.4 \ (\mathrm{W/(m\ °C)}) \ (-80 \le \theta \le 0) \end{cases} \tag{8}$$

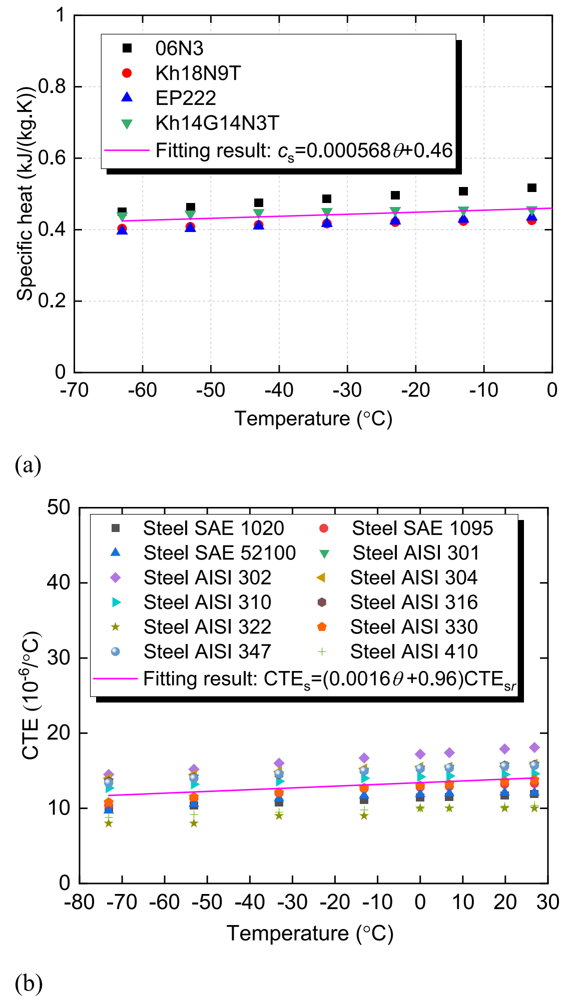

Fig. 5. Low temperature models of the thermal properties of steel: (a) Specific heat, (b) CTE.

Table 4
Thermal properties of the CFRP at different temperatures.

θ (°C)	ρ_P (kg/m^3)	CTE$_P$ (°C^{-1})	λ_P (W/(m °C))	c_P (kJ/(kg °C))
−80 to 0			1.4	1.25
20			1.356	1.308
40	1600	0	1.312	1.367
60			1.268	1.425
80			1.224	1.484

$$c_P = \begin{cases} 1.25 + \dfrac{0.95}{325}\theta \ (\mathrm{kJ/kg\ °C}) \ (0 \le \theta \le 80) \\ 1.25 \ (\mathrm{kJ/kg\ °C}) \ (-80 \le \theta \le 0) \end{cases} \tag{9}$$

2.2. Temperature effect mechanism on the component

Based on Section 2.1 and the specific structure of the component, the mechanism of the temperature effect on the component is illustrated in Fig. 6. Two typical ideal boundary conditions are considered.

The physical change process of the component with temperature change is explained in Fig. 6(a), which takes the temperature increase as an example. In the case that one end is movable and the other one is fixed, as the temperature increases, there is no thermal deformation of the CFRP due to its zero CTE, but the steel column and the prestressing

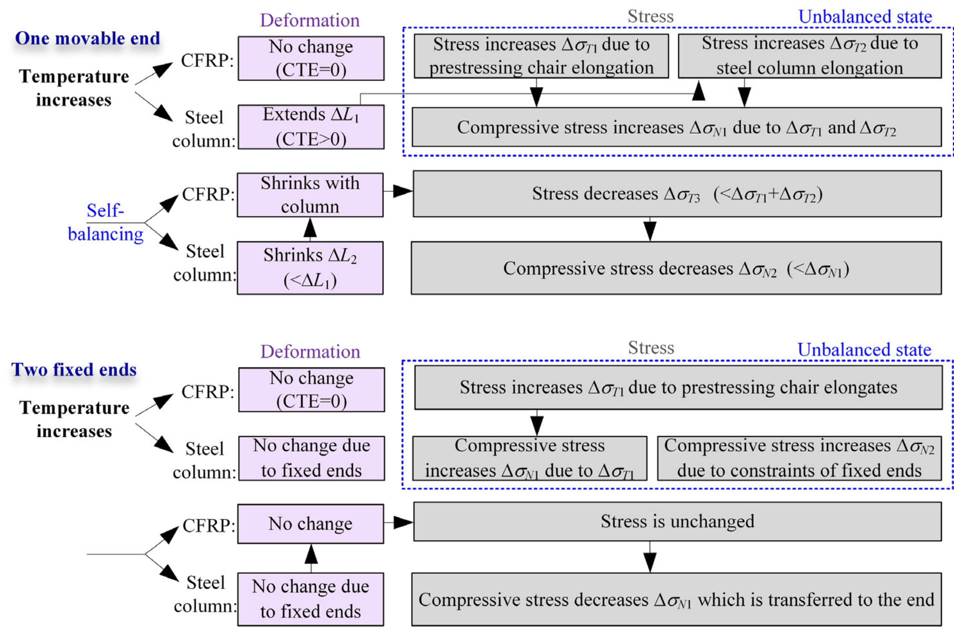

(a)

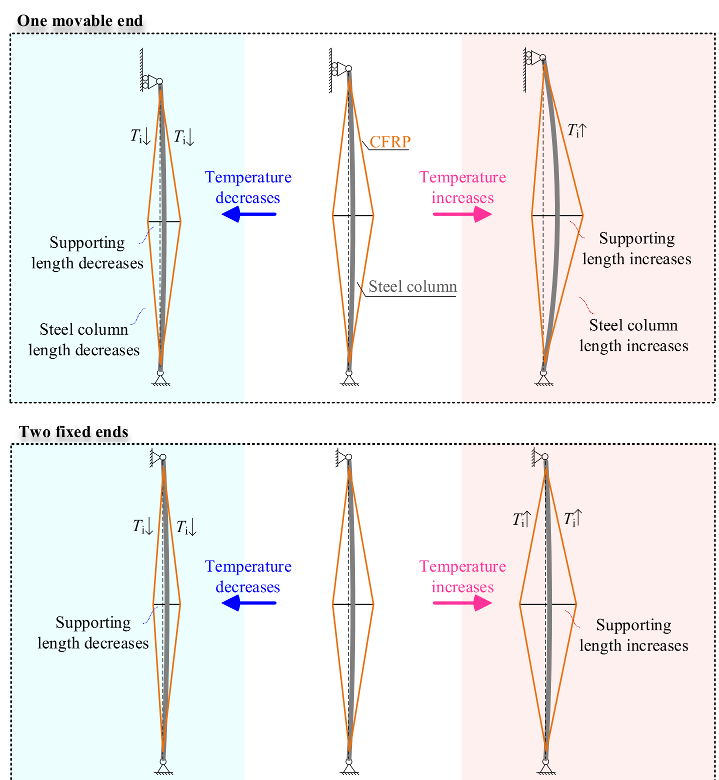

(b)

Fig. 6. Mechanism of the temperature effect on the component: (a) Physical change process (taking increasing temperature as an example), (b) Schematic diagram of the deformation change (not to scale).

chair elongate due to the positive CTE of steel. Therefore, the CFRP stress tends to increase $\Delta\sigma_{T1}$ and $\Delta\sigma_{T2}$ due to the elongation of the steel column and prestressing chair, respectively, which will lead to an increase in the steel column compressive stress ($\Delta\sigma_{N1}$). Because the steel column's stiffness is not infinite, there is a self-balancing process. In such a process, the steel column shrinks ΔL_2 ($<\Delta L_1$), and the CFRP shrinks with the steel column. Meanwhile, the CFRP stress decreases $\Delta\sigma_{T3}$ ($<(\Delta\sigma_{T1}+\Delta\sigma_{T2})$), and the steel column compressive stress decreases $\Delta\sigma_{N2}$ ($<\Delta\sigma_{N1}$). The compression of the prestressing chair in the self-balancing process is negligible. Compared with the initial state, after the temperature increases, the steel column and prestressing chair length increase; the CFRP tensile stress increases $\Delta\sigma_{T1}+\Delta\sigma_{T2}-\Delta\sigma_{T3}$, and

Table 5
The details of the typical specimen.

A_s (mm^2)	A_P (mm^2)	I_s (mm^4)	λ	L (mm)	L_c (mm)	a (mm)	Initial geometric imperfection (mm)	Residual stress (MPa)
1220	150	2.87×10^5	140	2150	2240	70	2.15 (0.1%L)	0

Notes: A_s and A_P are the section areas of steel and CFRP, respectively. I_s is the inertia moment of the weak axis of the steel section. λ is the column slenderness. L and L_c are the length and calculation length of the steel column, respectively. a is the supporting length of the prestressing chair at the midspan.

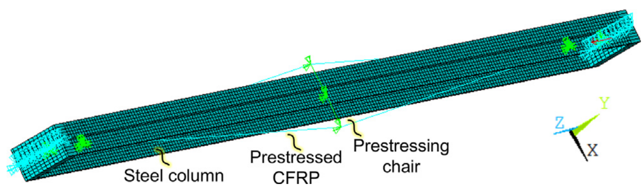

Fig. 7. FE modeling of the prestressed CFRP-reinforced steel column.

the steel column compressive stress increases $\Delta\sigma_{N1}$–$\Delta\sigma_{N2}$ (regardless of the influence of lateral deformation of the column).

In the case that two ends of the component are fixed, which forms a statically indeterminate system, as the temperature increases, both the CFRP and steel column have no thermal deformations, but the prestressing chair elongates. The CFRP stress increases $\Delta\sigma_{T1}$ due to this elongation, which results in an increase in the steel column's compressive stress ($\Delta\sigma_{N1}$); meanwhile, the steel column is constrained by the fixed ends but tends to elongate, which forms another compressive stress $\Delta\sigma_{N2}$. Because the component with such boundary conditions is an indeterminate structure, $\Delta\sigma_{N1}$ will be transferred to the ends. Therefore, compared with the initial state, after the temperature increases, the steel column length is unchanged, and the prestressing chair and CFRP length increase; the CFRP tensile stress increases $\Delta\sigma_{T1}$, and the steel column compressive stress increases $\Delta\sigma_{N2}$.

More specifically, with the variation in temperature, schematic diagram of the deformation change in the component is shown in Fig. 6(b). Considering such a complex process as well as the change in materials with temperature change (Section 2.1) and the real constraints, the temperature effect on the reinforced column is studied by FEM in the following sections.

3. Buckling analysis at steady state

This section studies the buckling behavior of the column at a certain temperature in the range of −80 °C to 80 °C. A typical case is used and the details are shown in Table 5. It is an I-section steel column with web/flange thickness of 5 mm and section height of 114 mm. The steel is hot-rolled; most residual stress was released due to manufacturing process [35], thus residual stress is set 0. The Euler load P_E of the column before reinforcement is 118.36 kN. One of the important factors determining the buckling capacity (P_b) of the reinforced column is the CFRP prestress (T_i) [35,48], where T_i refers to the prestress value after the self-balancing of the reinforced column. Thus, this section focuses on the influence of temperature on this T_i and P_b relationship, which shows the difference in buckling capacities for the same column at different temperatures. Meanwhile, the influence of temperature on the deformation/stiffness/yielding of the columns is also revealed.

3.1. Finite element modeling

Finite element (FE) modeling using ANSYS 11.0 was basically the same as that in Ref. [35], as shown in Fig. 7. The steel column and the CFRP were meshed using SOLID45 and LINK10 elements, respectively. Two hinged supports were simulated, and a compressive load was applied on one end of the column in the axial direction. 0.1%L initial geometric imperfection based on the first-order buckling mode were

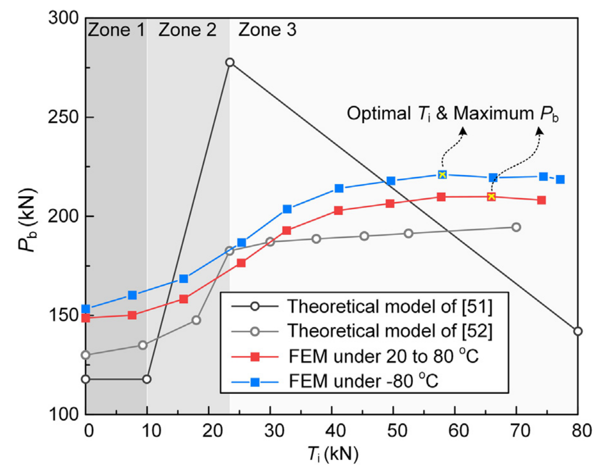

Fig. 8. T_i–P_b relationship when the column is loaded at a certain temperature.

applied. Then an arc length method was used to conduct a nonlinear buckling analysis. For more details, refer to [35].

This FE model at room temperature has been verified by many experiments [35], and this paper conducted analysis of such columns at different temperatures using the validated model. The temperature effect on the reinforced column includes two parts. The first is temperature effect on the materials, and the mechanical properties of steel and CFRP at different temperatures were set according to the solid data in Section 2.1. The second is temperature effect on the component analyzed in Section 2.2, which is based on the thermal expansion and contraction effect. It is determined by the thermal properties of steel and CFRP, which were also set according to the solid data in Section 2.1. Thus, the analysis result by the FE model in this paper is reliable [49,50].

As stated in Refs. [35,48], with the change in T_i, P_b obviously changes. Therefore, we set the CFRP prestress before the column self-balancing as an arithmetic sequence from 0 to 540 MPa and thus have T_i as 0, 7.6, 15.9, 25.3, 32.7, 41.1, 49.5, 57.8, 65.9, and 74.1 kN, and conducted 21 tests to obtain the influence of temperature on the T_i–P_b relationship. In addition, typical force–deformation curves were obtained, which show the temperature effect on the yield point and stiffness of specimens.

3.2. Results and discussion

The results of temperature effect on T_i–P_b relationship are shown in Figs. 8–9. At room temperature, the theoretical model by Hafez et al. [51] shows a three-zone tendency for such columns under ideal conditions; FEM results and the theoretical model by Hu et al. [52] reflect the influence of T_i on P_b under real conditions, which have very similar tendencies. From Fig. 8, the following findings are obtained. (1) High temperature: Due to the very limited change in E_s, E_P, f_y and f_u from 20 to 80 °C and the fact that the strength of CFRP is very large and is not the controlling factor of P_b, the T_i–P_b relationship is almost the same from 20 to 80 °C and can be represented by one line. (2) Low temperature: Due to the increase in E_s, E_P, f_y and f_u from 20 to −80 °C, the T_i–P_b relationship at a low temperature is different

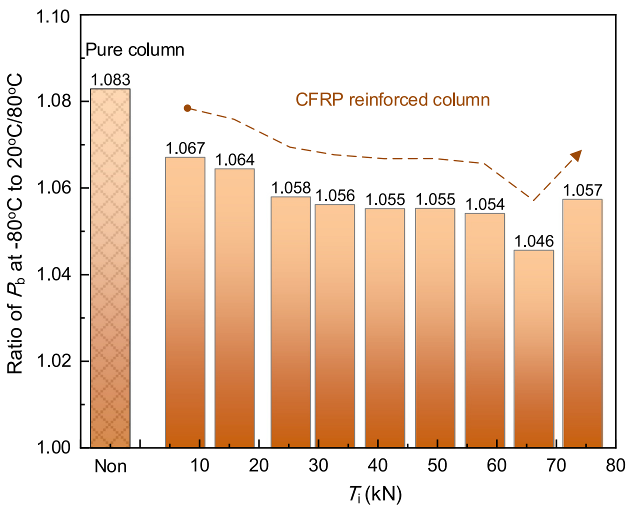

Fig. 9. The ratio of P_b at −80 °C to 20 °C/80 °C.

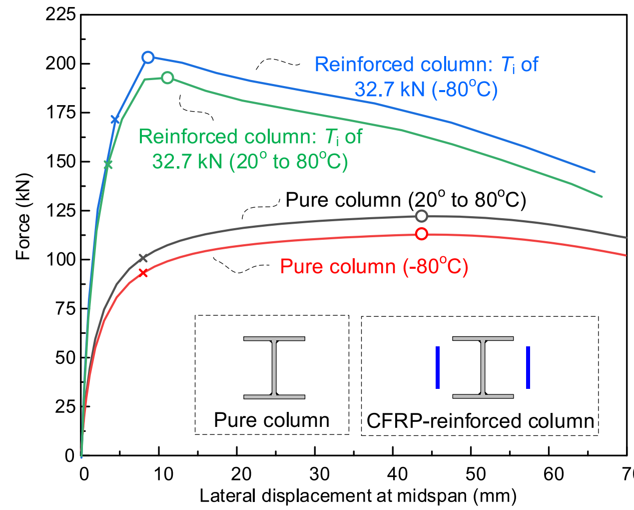

Fig. 10. Force-lateral displacement curves at different temperatures when the column is loaded at a certain temperature.

from that at room temperature. Thus, a different line representing the relationship at −80 °C is shown in Fig. 8. For temperatures between 20 and −80 °C, the T_i–P_b relationship is between the two lines. At the same value of T_i, when the temperature drops from 20 °C/80 °C to −80 °C, there is a 3% to 7% increase in P_b, and the optimal value of T_i, which corresponds to the maximum value of P_b, is shifted from 66 kN to 58 kN. This is because steel has an 8.3% increase in E_s and a 9.1% increase in f_y while CFRP only has a 1.2% increase in E_P.

Additionally, the ratio of P_b at −80 °C and 20 °C/80 °C when T_i varies is shown in Fig. 9. Fig. 9 excludes the reinforced situation of $T_i = 0$ because FRP is not prestressed and thus does not fully work. The temperature effect is more obvious on the pure column (ratio > 1.08) than on the reinforced column. This implies that the temperature effect is weakened by the prestressed CFRPs. When focusing on the reinforced column with different T_i values, the following conclusions are found. As T_i increases, this ratio gradually decreases when T_i is not very large, which proves that a highly prestressed CFRP works more efficiently against the temperature effect; however, when T_i surpasses its optimal value at room temperature (66 kN), this ratio suddenly becomes large, which is because P_b at room temperature is small in this situation.

Fig. 10 shows four typical force-lateral displacement curves of pure and reinforced steel columns at −80 °C and 20 °C/80 °C. The lateral displacement was determined by the node at the neutral axis of the I-section at the midspan of the specimen. It can be seen that in addition to buckling capacity P_b, the yield point and stiffness are also influenced by the temperature with a similar tendency.

4. Buckling analysis considering temperature change

This section studies the buckling behavior of the column considering temperature change. To simulate the real behavior of the column when the temperature changes, compressive preloading is first added to the column, and then thermal loading reflecting the temperature change is added to the column. Based on this model, the lateral displacement, axial displacement, CFRP and steel stress change and the failure mechanism can be obtained.

4.1. FE modeling

The basic model is the same as that in Section 3.1, except that the boundary conditions are as follows: a compression load named P_{pre} was applied to the column at 20 °C, and then thermal boundary conditions from the heat transfer analysis were applied to the specimens [37]. Two thermal change situations are included: one is from 20 °C to 80 °C, and the other is from 20 °C to −80 °C. Because the thicknesses of FRP and steel of this column are very small, the temperature gradient was not considered; in addition, thermal convection, thermal radiation, and heat conduction are not considered in this paper; thus, the whole specimen is set as the same temperature. The material parameters at different temperatures are based on Section 2.1. Three typical specimens with different CFRP prestress values were considered. The specimen of T_i = 7.56 kN refers to a small value of CFRP prestress, which is in the first zone in Fig. 8 [51]. The specimens of T_i = 32.67 (smaller than the optimal value of T_i) and 57.78 kN (the optimal value) refer to middle and large values of T_i, respectively, which are both in the third zone in Fig. 8 [51].

For each specimen, P_{pre} was set as 0.1, 0.5 and 1.0 times P_E, thus forming 9 cases. Therefore, the ratio of P_{pre} to P_b for every case is different, as shown in Tables 6–7. P_{pre}/P_b reflects the utilization rate of the bearing capacity of the column and is a key factor in engineering. Therefore, studying the effect of temperature change on the buckling behavior of reinforced columns with different values of P_{pre}/P_b is of practical engineering significance.

4.2. Results and discussion

4.2.1. Results

The results are shown in Tables 6–7 and Figs. 11–15. The positive values of CFRP stress refer to tensile stress; the positive values of steel stress refer to compressive stress; the positive and negative lateral displacements depend on the coordinate system, as shown in Fig. 7; and the positive axial displacement of the steel column refers to the compressive displacement.

(1) General tendency

First, after the self-balancing of the prestressed CFRP-reinforced steel column, the axial compressive displacement and the steel compressive stress increase from zero, and the CFRP tensile prestress on both sides simultaneously decreases. Second, preloading P_{pre} is added; therefore, lateral displacement occurs, the CFRP prestress of the concave and convex sides becomes different, the axial compressive displacement increases, and the steel stress also changes. Therefore, the initial values of the lateral and axial displacements, CFRP and steel stresses at 20 °C are not zero.

When the temperature starts to change, the following phenomenon occurs. Two typical deformations referring to high and low temperatures are shown in Fig. 11. From room to high temperature, the column

Table 6
CFRP stress of specimens when temperature changes.

Case No.	T_i (kN)	P_{pre}/P_E	P_{pre}/P_b	Concave (MPa)			Convex (MPa)		
				−70 °C	20 °C	80 °C	−70 °C	20 °C	80 °C
1		0.1	0.08	0 (−100%)[a]	80.2	155.4 (+94%)	0 (−100%)	82.4	218.4 (+165%)
2	7.56	0.5	0.39	0 (−100%)	50.2	76.0 (+51%)	0 (−100%)	59.4	216.0 (+264%)
3		1.0	0.79	0 (−100%)	12.8	0 (−100%)	1.8 (−94%)	30.7	352.6 (+1049%)
4		0.1	0.06	71.7 (−68%)	223.7	301.0 (+35%)	73.8 (−68%)	227.1	357.0 (+57%)
5	32.67	0.5	0.31	42.8 (−78%)	193.6	225.6 (+17%)	54.5 (−73%)	204.2	352.7 (+73%)
6		1.0	0.61	2.3 (−98%)	151.1	49.9 (−67%)	34.6 (−81%)	180.6	380.5 (+111%)
7		0.1	0.06	215.2 (−36%)	336.8	425.3 (+26%)	218.7 (−36%)	342.2	500.6 (+46%)
8	57.78	0.5	0.28	186.0 (−45%)	337.1	301.3 (−11%)	199.8 (−43%)	349.0	501.6 (+44%)
9		1.0	0.56	143.8 (−51%)	292.7	109.2 (−63%)	180.8 (−44%)	324.8	529.7 (+63%)

[a]Form: Absolute value (relative change).

Table 7
Displacement of specimens when temperature changes.

Case No.	T_i (kN)	P_{pre}/P_E	P_{pre}/P_b	Axial displacement (mm)			Lateral displacement (mm)		
				−70 °C	20 °C	80 °C	−70 °C	20 °C	80 °C
1		0.1	0.08	1.9	−0.3	−1.5	0.2	0.1	3.9
2	7.56	0.5	0.39	2.3	0.0	−0.9	1.8	0.5	8.2
3		1.0	0.79	3.1	0.4	2.2	15.9	0.9	36.1
4		0.1	0.06	2.1	0.0	−1.1	0.1	0.2	3.4
5	32.67	0.5	0.31	2.4	0.3	−0.5	0.6	0.6	7.3
6		1.0	0.61	2.8	0.8	0.8	1.7	1.6	18.8
7		0.1	0.06	2.4	0.3	−0.7	0.2	0.3	4.5
8	57.78	0.5	0.28	2.7	0.7	0.3	0.8	0.7	11.6
9		1.0	0.56	3.1	1.1	1.9	2.0	1.8	23.7

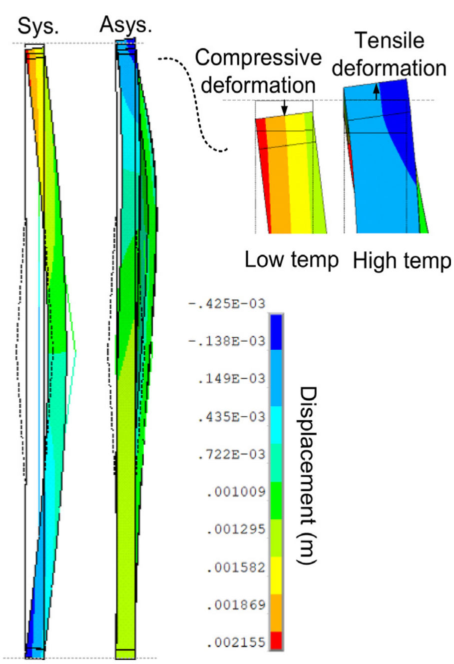

Fig. 11. Typical deformations under low and high temperatures in FEM.

tends to extend, and the deformation is first symmetric and global and finally changes to local and asymmetric deformation. From room temperature to low temperature, the column tends to shrink, and the deformation is always symmetric and global. More specific details are presented as follows.

For the high temperature effect, from 20 to 80 °C, there is a temperature that divides the whole changing process into two parts, which is defined as a turning-point temperature (as shown in Figs. 12–14). Main characteristics of stress and displacement changes before/at/after turning-point temperature are summarized in Table 8. Specifically, before the temperature reaches the turning-point temperature, the axial displacement is mainly controlled by the "thermal expansion and contraction effect" rather than the CFRP stress. At this stage, when the temperature increases, the steel column length increases; therefore, the compressive axial displacement of the steel column decreases to zero and even becomes negative (i.e., tensile displacement), the CFRP is stretched, and its stress increases rapidly. This increase in CFRP stress leads to a slow increase in steel stress, and the lateral displacement is still almost unchanged, especially for a small P_{pre}.

After the turning-point temperature, the axial displacement is controlled by both the "thermal expansion and contraction effect" and the large CFRP stress. Due to the large CFRP stress at this stage, the tensile axial displacement increases if P_{pre} is small, but it increases for a while and then decreases if P_{pre} is large. At this stage, the difference in CFRP stresses of the two sides becomes obvious; the convex CFRP stress continues to increase and thus has a large value; the concave CFRP stress starts to increase at a very slow speed when T_i is small (7.56 kN) or P_{pre} is small ($0.1P_E$) and starts to decrease when T_i and P_{pre} are both large. Due to this large CFRP stress, the lateral displacement rapidly increases, and asymmetric local buckling of the flange occurs (Fig. 11), which causes a sudden change in the steel stress and a nonmonotonic change afterward.

For the low temperature effect, from −80 to 20 °C, for specimens with a middle/large value of T_i (T_i = 32.67 and 57.78 kN), the general tendency is similar to that from 20 °C to the turning-point temperature, as described above; this trend is also due to the change of material properties. When temperature becomes lower, elastic modulus increases, which leads to a stress reduction of steel and CFRP. However, the low temperature effect of the specimen with a small value of T_i (T_i = 7.56 kN) is different, as shown in Fig. 12. Specifically, when the temperature decreases from 20 to −80 °C, the CFRP stresses gradually decrease to zero (i.e., the CFRP becomes slack). After the CFRP stresses decreases to a certain small value, the steel column loses lateral supports; therefore, there is an increase in the lateral displacement when the temperature decreases, which is especially obvious for specimens with a large P_{pre}.

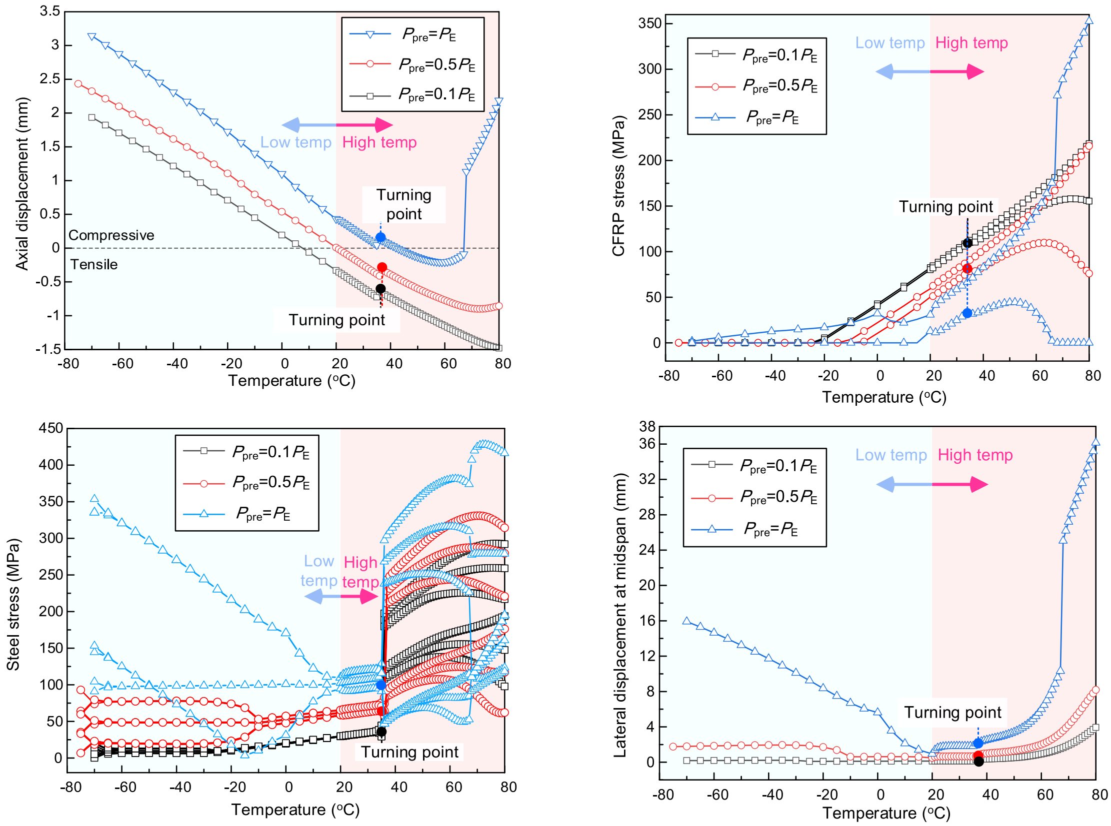

Fig. 12. Results for specimens with T_i = 7.56 kN when temperature changes.

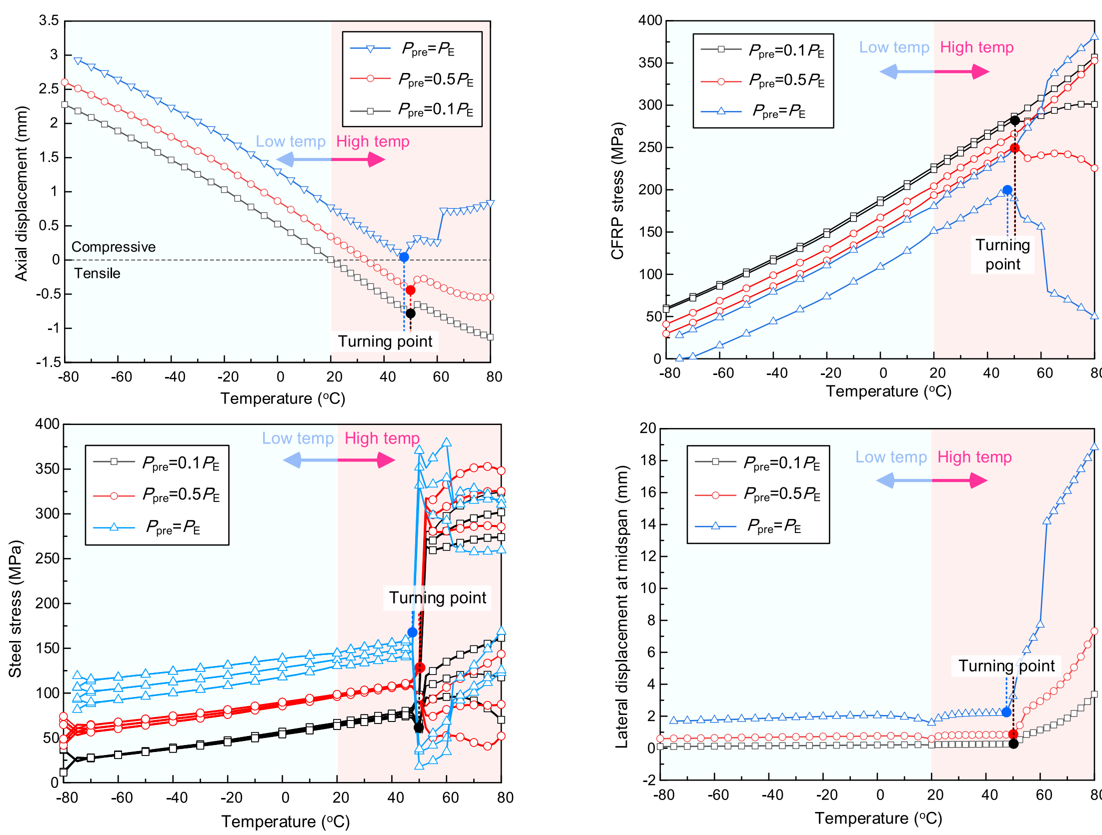

Fig. 13. Results for specimens with T_i = 32.67 kN when temperature changes.

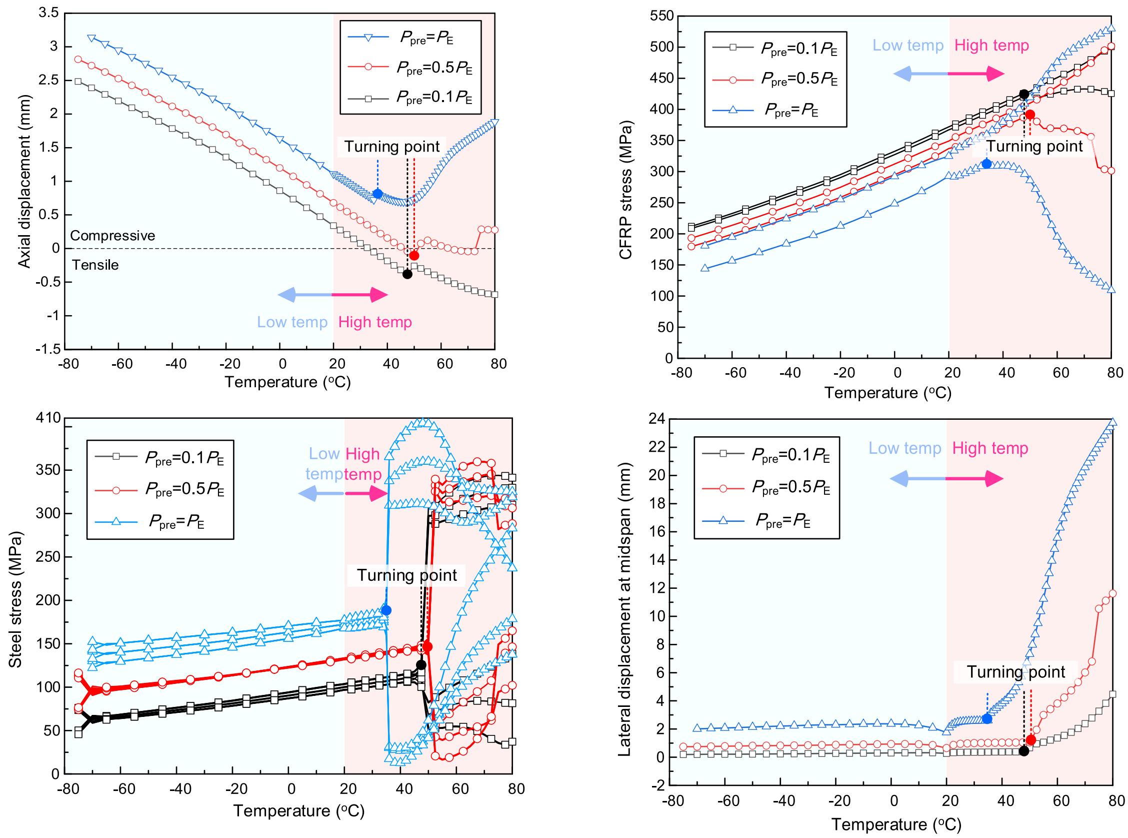

Fig. 14. Results for specimens with T_i = 57.78 kN when temperature changes.

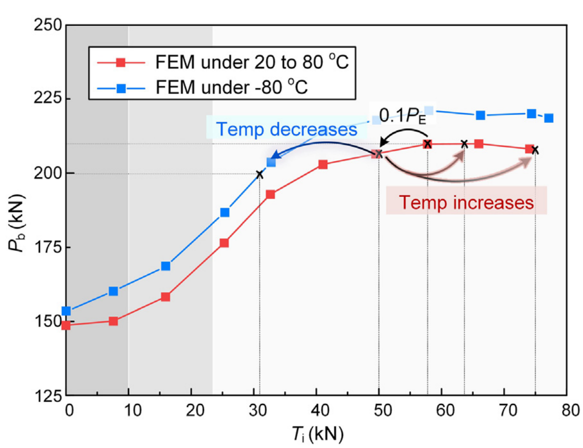

Fig. 15. A typical CFRP prestress change in the T_i–P_b relationship.

This increase in lateral displacement causes a large change in steel stresses; that is, the convex side steel stress increases and the concave side decreases, and the difference in steel stresses on the concave and convex sides becomes very large.

Furthermore, when considering temperature effect, because the overall stress state is affected by the temperature, there is a possibility of the prestressed columns, with longer supporting length or stiffer FRPs, suffering from buckling mode interactions [32]. Thus, there are two situations. (1) For a column whose buckling loads for Modes 1 and 2 (i.e., symmetric and antisymmetric) vary widely, symmetric buckling occurs at room temperature, and interactive buckling does not occur after temperature change; (2) for a column whose buckling loads for Modes 1 and 2 are relatively close, symmetric buckling occurs at room temperature, and interactive buckling occurs after a small temperature change. For the studied column, because its supporting length is small (70 mm), it belongs to situation (1).

(2) Change in stress and displacement

The absolute and relative changes in stress and displacement are important for determining the buckling capacity of the columns after a temperature change, which are shown in Tables 6–7.

From 20 to −70 °C, for specimens with a middle/large value of T_i (32.67 and 57.78 kN), the absolute change in CFRP stress is large, which is 121.6–153.3 MPa (i.e., Cases 4–9), and the maximum value is in Case 4. The increase in axial compressive displacement of all the specimens is significant (i.e., 2.0–2.7 mm), and the maximum displacement is in Case 3. Most specimens have an increase in lateral displacement (i.e., varying from 0 to 15.0 mm), and the maximum displacement is in Case 3, while Cases 4 and 7 demonstrate a 0.1 mm decrease.

From 20 to 80 °C, the CFRP stress change can be as high as 321.9 MPa (i.e., convex side of Case 3). Most specimens show a decrease in axial compressive displacement (i.e., 0.4–1.2 mm), and the maximum displacement is in Case 1, while the specimens with P_{pre} = P_E exhibit an increase in compressive displacement in the range of 0.1–1.8 mm, and the maximum displacement is in Case 3. All specimens demonstrate an increase in lateral displacement (i.e., 3.2–35.2 mm), and the maximum displacement is in Case 3.

4.2.2. Discussion

(1) Influence of P_{pre} on thermal sensitivity

Before adding the thermal loading, with the same T_i, a larger P_{pre} leads to a larger lateral/axial displacement. Thus, a larger P_{pre} leads to a larger drop in the initial CFRP stress and a higher compressive steel stress because of this larger axial compression, and a larger difference in the stresses of the concave- and convex-side CFRPs and a larger

Table 8
Main characteristics of stress and displacement changes when temperature increases before/at/after turning-point temperature.

	Before turning-point temperature	**At** turning-point temperature	**After** turning-point temperature
Steel stress	a slow increase	a sudden change	a nonmonotonic change
CFRP stress	a very small and unchanged difference of the two sides	/	an increasingly obvious difference of the two sides
Axial displacement	/	a sudden change	/
Lateral displacement	a limited change	/	a rapidly increasing

difference in stresses of the concave- and convex-sides of the steel section because of this larger lateral displacement.

In terms of thermal sensitivity, the high temperature effect on specimens with a larger P_{pre} is more significant, while the low temperature effect is almost the same for all cases. This is because high temperature causes CFRP stress increasing, which easily leads to nonlinear buckling of the specimens under a large P_{pre}. Therefore, the stress and displacements of specimens with a large P_{pre} are more thermally sensitive.

(2) Influence of T_i on thermal sensitivity

Before adding the thermal condition, with the same P_{pre}, a larger T_i contributes to a larger axial displacement because of the larger vertical component of force and a smaller lateral displacement because of the stronger lateral support by CFRP. In addition, because T_i is no larger than the optimal value for all the cases, a larger T_i contributes to a higher buckling capacity and leads to a lower value of P_{pre}/P_b.

In terms of thermal sensitivity, as shown in Tables 6–7, in general, for cases with a larger value of T_i, when the temperature changes, the CFRP stress change is larger, while the axial and the lateral displacements do not show a unified rule. Therefore, the stress of specimens with a larger T_i is more thermally sensitive, but the thermal sensitivity of displacement does not have a clear relationship with T_i from this view. However, from another view, due to the relatively lower value of turning-point temperature for specimens with low T_i (7.56 kN), it can be inferred that a high temperature could easily have an impact on specimens with higher values of T_i. Furthermore, the turning-point temperatures of specimens with T_i = 7.56 kN are almost the same (i.e., 35 °C); those with T_i = 32.67 kN vary slightly with different values of P_{pre} (46 °C for P_E, 50 °C for 0.1 and 0.5P_E); those with T_i = 57.78 kN vary greatly with different values of P_{pre} (35 °C for P_E, 50 °C for 0.1 and 0.5P_E). Therefore, for specimens with a higher T_i, their turning-point temperatures are more sensitive to the preloading.

5. Residual buckling capacity after temperature change

Combined with Sections 3 and 4, the residual buckling capacity (i.e., the total buckling capacity P_b minus the P_{pre}) after a temperature change can be obtained.

Taking Case 7 in Tables 6–7 as an example, before adding P_{pre}, T_i is 57.78 kN; after adding P_{pre} of 0.1P_E, T_i decreases to approximately 51 kN. A typical CFRP prestress change with temperature change is drawn in the T_i–P_b relationship, as shown in Fig. 15. T_i of both sides decreases to approximately 31 kN if the temperature decreases to −80 °C; T_i of the concave and convex sides increase to 64 and 75 kN, respectively, if the temperature increases to 80 °C. P_b of the column is sensitive to T_i, and the temperature change after adding P_{pre} also causes changes in the steel stress, displacements, and material properties. Therefore, the temperature change after adding P_{pre} has an obvious influence on the total and residual buckling capacity of the column.

To further clarify this point, an additional compressive loading is added to this specimen after the temperature change. The force–displacement curve during the whole process is shown in Fig. 16 by the gray line with square symbols. A red line with circle symbols representing the same specimen that is loaded by compressive loading directly is also drawn for comparison (referred to as the normal case). The total buckling capacity decreases by 20 kN if the temperature

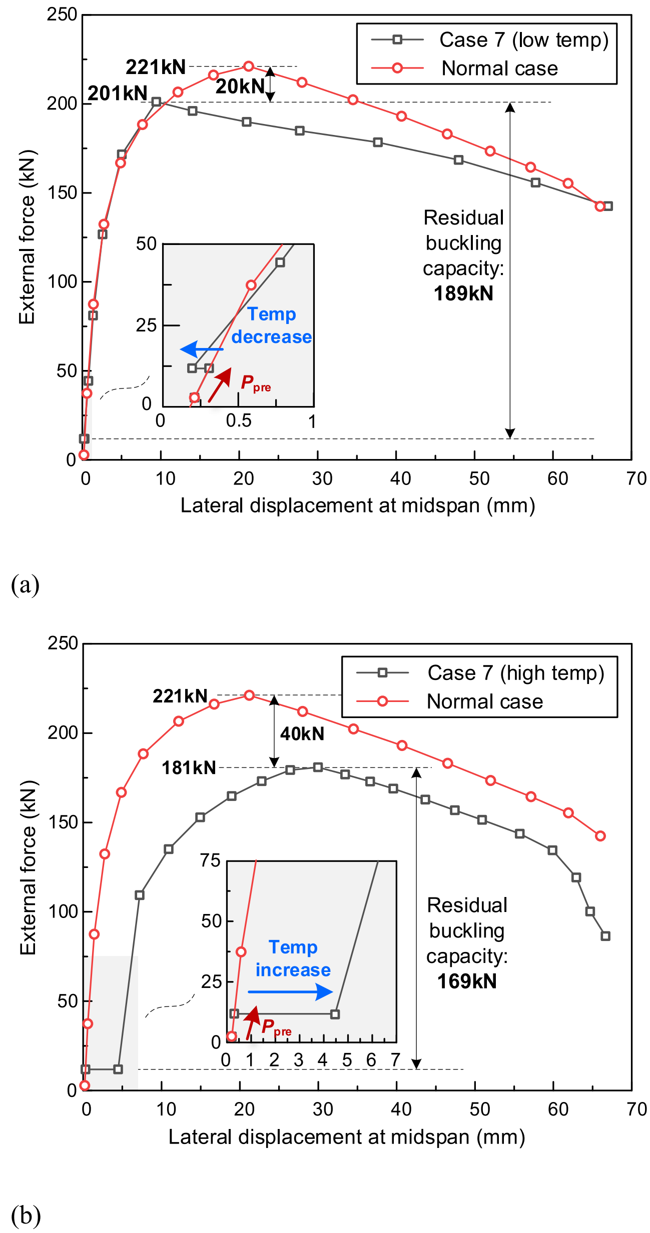

Fig. 16. Force–displacement curves under preloading-temperature change-loading: (a) Temperature decreasing, (b) Temperature increasing.

decreases to −80 °C after preloading, and the residual buckling capacity is 189.4 kN. When the temperature increases to 80 °C after preloading, due to the large lateral displacement caused by the temperature, the total buckling capacity decreases more significantly (i.e., 40 kN, 18% of the total buckling capacity), and the residual buckling capacity is only 169.1 kN.

In conclusion, the temperature change leads to a large drop in the buckling behavior of the prestressed CFRP-reinforced column. Based on results of Section 4.2, the specimens with a higher T_i have a greater influence on the turning-point temperatures; the lateral displacement of specimens with higher P_{pre} increases more rapidly after the turning-point temperatures. This indicates that when designing the columns with a high value of T_i or P_{pre} in regions with large temperature differences between the four seasons, a reduction coefficient of buckling capacity could be introduced to consider the temperature effect.

6. Conclusions

The following conclusions can be drawn:

(1) When the column is loaded at a certain temperature between −80 to 80 °C, high temperature does not have an obvious influence on its buckling capacity. However, when the temperature dropped from 20 °C to −80 °C, the buckling capacity increased 3%–7%, and the optimal CFRP prestress decreased; the prestressed CFRP can mitigate the temperature effect, and CFRP with T_i closer to its optimal value works more efficiently.
(2) When the column is preloaded and the temperature changes from 20 to 80 °C, a turning-point temperature exists. Before the turning-point temperature, the deformation is symmetric and global; when the temperature increases, the CFRP stress increases rapidly, the steel stress increases slowly, and the lateral displacement is almost unchanged. After that, the difference in the CFRP stresses on the two sides becomes significant, the lateral displacement rapidly increases, and the asymmetric local buckling of the flange occurs.
(3) When the column is preloaded and the temperature changes from 20 to −80 °C, the deformation is symmetric and global. For most specimens, the CFRP stress decreases rapidly, the steel stress decreases slowly and the lateral displacement is almost unchanged. However, for specimens with a small CFRP prestress, after the CFRP stresses decrease to a small value, the steel column loses lateral supports. Therefore, the lateral displacement may increase suddenly, and the steel stress undergoes a large change.
(4) The influences of preloading and CFRP prestress on the thermal sensitivity of such columns are obtained. The high temperature effect on specimens with a larger P_{pre} or T_i is more significant. In addition, for specimens with a larger T_i, their turning-point temperatures are more sensitive to P_{pre}.
(5) The temperature change leads to a large decrease in the buckling capacity (e.g., 18%). This decrease is more significant with temperature increasing rather than decreasing. It is recommended that such temperature effect be considered in design under extreme conditions.

CRediT authorship contribution statement

Lili Hu: Writing – review & editing, Writing – original draft, Software, Methodology, Investigation. **Xu Liang:** Writing – original draft, Investigation, Formal analysis, Data curation. **Peng Feng:** Writing – review & editing, Validation, Conceptualization. **Hai-Ting Li:** Writing – review & editing, Validation, Methodology.

Declaration of competing interest

The authors declare that they have no known competing financial interests or personal relationships that could have appeared to influence the work reported in this paper.

Data availability

Data will be made available on request.

Acknowledgments

This research was supported by the Natural Science Foundation of Shanghai, China (No. 23ZR1430000) and Young Elite Scientists Sponsorship Program by CAST, China (No. 2022QNRC001).

References

[1] World Facts, The coldest temperatures ever recorded on earth, https://www.worldatlas.com/articles/the-coldest-temperatures-ever-recorded-on-earth.html.
[2] M.C. Serreze, G.B. Roger, The Arctic Climate System, Cambridge University Press, New York, 2009.
[3] World Facts, What was the hottest temperature ever recorded? https://www.worldatlas.com/articles/the-hottest-temperatures-ever-recorded-in-the-world.html.
[4] Spain sizzles as temperatures soar to 43 °C in first heatwave of the year. https://www.breakingnews.ie/world/spain-sizzles-as-temperatures-soar-to-43c-in-first-heatwave-of-the-year-1318660.html.
[5] National weather service, Climate Prediction Center, USA, https://www.cpc.ncep.noaa.gov/.
[6] National Meteorological Observatory, China. http://www.nmc.cn.
[7] D.S. Chen, H.L. Qian, H.J. Wang, et al., Experimental and numerical investigation on the non-uniform temperature distribution of thin-walled steel members under solar radiation, Thin-Walled Struct. 122 (2018) 242–251, http://dx.doi.org/10.1016/j.tws.2017.10.018.
[8] X.Y. Cao, G. Wu, J.W. Ju, Seismic performance improvement of existing RCFs using external PT-PBSPC frame sub-structures: Experimental verification and numerical investigation, J. Build. Eng. 46 (2021) 103649, http://dx.doi.org/10.1016/j.jobe.2021.103649.
[9] X.L. Zhao, FRP-Strengthened Metallic Structures, CRC Press, Boca Raton, 2013.
[10] J.Z. Shi, X. Wang, Z.S. Wu, X. Wei, X.G. Ma, Long-term mechanical behaviors of uncracked concrete beams prestressed with external basalt fiber-reinforced polymer tendons, Eng. Struct. 262 (2022) 114309, http://dx.doi.org/10.1016/j.engstruct.2022.114309.
[11] J.S. Fan, C. Liu, Y.F. Liu, Review of temperature distribution and temperature effects of steel-concrete composite girder bridges in China, China J. Highw. Transp. 33 (4) (2020) 1–13, (in chinese) https://10.19721/j.cnki.1001-7372.2020.04.001.
[12] R.A. Imbsen, D.E. Vandershaf, Thermal Effects in Concrete Bridge Superstructures, National Research Council, Washington DC, 1984.
[13] F.A. Branco, P.A. Mendes, Thermal actions for concrete bridge design, J. Struct. Eng. 119 (8) (1993) 2313–2331, https://ascelibrary.org/doi/10.1061/(ASCE)0733-9445(1993)119:8(2313).
[14] J. Scheer, Failed Bridges: Case Studies, Causes and Consequences, John Wiley & Sons, New York, 2011.
[15] E. Ghafoori, M. Motavalli. Normal, High and ultra-high modulus carbon fiber reinforced polymer laminates for bonded and un-bonded strengthening of steel beams, Mater. Des. 67 (2015) 232–243, http://dx.doi.org/10.1016/j.matdes.2014.11.031.
[16] L.L. Hu, P. Feng, W.Y. Gao, Y.H. Wang, Flexural behavior of light steel purlins reinforced by prestressed CFRP laminates, Thin-Walled Struct. 174 (2022) 109125, http://dx.doi.org/10.1016/j.tws.2022.109125.
[17] A. Shaat, A.Z. Fam, Slender steel columns strengthened using high-modulus CFRP plates for buckling control, J. Compos. Constr. 13 (1) (2009) 2–12, https://ascelibrary.org/doi/10.1061/(ASCE)1090-0268(2009)13:1(2).
[18] P. Feng, Y.H. Zhang, Y. Bai, L.P. Ye, Strengthening of steel members in compression by mortar-filled FRP tubes, Thin-Walled Struct. 64 (3) (2013) 1–12, http://dx.doi.org/10.1016/j.tws.2012.11.001.
[19] P. Colombi, Reinforcement delamination of metallic beams strengthened by FRP strips: fracture mechanics based approach, Eng. Fract. Mech. 73 (2006) 1980–1995, http://dx.doi.org/10.1016/j.engfracmech.2006.03.011.
[20] L.L. Hu, Y.Y. Wang, P. Feng, H.T. Wang, H.L. Qiang, Debonding development in cracked steel plates strengthened by CFRP laminates under fatigue loading: experimental and boundary element method analysis, Thin-Walled Struct. 166 (2021) 108038, http://dx.doi.org/10.1016/j.tws.2021.108038.
[21] L.A. Bisby, Fire Behaviour of Fibre-Reinforced Polymer (FRP) Reinforced or Confined Concrete, Queen's University, Ontario, Canada, 2003.
[22] W.Y. Wang, K. Wang, V. Kodur, B. Wang, Mechanical properties of high-strength Q690 steel at elevated temperature, J. Mater. Civ. Eng. 30 (2018) 04018062, https://ascelibrary.org/doi/10.1061/(ASCE)MT.1943-5533.0002244.
[23] J.B. Yan, Y.L. Luo, X.C. Lin, Y.B. Luo, L.X. Zhang, Effects of the Arctic low temperature on mechanical properties of Q690 and Q960 high-strength steels, Constr. Build. Mater. 300 (2021) 124022, http://dx.doi.org/10.1016/j.conbuildmat.2021.124022.
[24] P. Feng, L.L. Hu, X.L. Zhao, L. Chen, S.H. Xu, Study on thermal effects on fatigue behavior of cracked steel plates strengthened by CFRP sheets, Thin-Walled Struct. 82 (2014) 311–320, http://dx.doi.org/10.1016/j.tws.2014.04.015.

[25] T.C. Nguyen, Y. Bai, X.L. Zhao, R. Al-Mahaidi, Mechanical characterization of steel/CFRP double strap joints at elevated temperatures, Compos. Struct. 93 (2011) 1604–1612, http://dx.doi.org/10.1016/j.compstruct.2011.01.010.

[26] H.C. Biscaia, P. Ribeiro, A temperature-dependent bond–slip model for CFRP-to-steel joints, Compos. Struct. 217 (2019) 186–205, http://dx.doi.org/10.1016/j.compstruct.2019.03.019.

[27] E. Ghafoori, A. Hosseini, R. Al-Mahaidi, X.L. Zhao, M. Motavalli, Prestressed CFRP-strengthening and long-term wireless monitoring of an old roadway metallic bridge, Eng. Struct. 176 (2018) 585–605, http://dx.doi.org/10.1016/j.engstruct.2018.09.042.

[28] E. Ghafoori, M. Motavalli, A. Nussbaumer, A. Herwig, G.S. Prinz, M. Fontanadet, Design criterion for fatigue strengthening of riveted beams in a 120-year-old railway metallic bridge using pre-stressed CFRP plates, Composites B 68 (2015) 1–13, http://dx.doi.org/10.1016/j.compositesb.2014.08.026.

[29] P. Feng, L.L. Hu, Steel columns strengthened/reinforced by prestressed CFRP strips: Concepts and behaviors under axial compressive loads, Compos. Struct. 217 (2019) 150–164, http://dx.doi.org/10.1016/j.compstruct.2019.03.038.

[30] L.L. Hu, P. Feng, Prestressed CFRP-reinforced steel columns under axial and eccentric compression, Compos. Struct. 268 (2021) 113940, http://dx.doi.org/10.1016/j.compstruct.2021.113940.

[31] D. Saito, M.A. Wadee, Numerical studies of interactive buckling in prestressed steel stayed columns, Eng. Struct. 31 (2) (2009) 432–443.

[32] D. Saito, M.A. Wadee, Post-buckling behaviour of prestressed steel stayed columns, Eng. Struct. 30 (5) (2008) 1224–1239.

[33] A.I. Osofero, M.A. Wadee, L. Gardner, Experimental study of critical and post-buckling behaviour of prestressed stayed columns, J. Construct. Steel Res. 79 (2012) 226–241.

[34] S.A.L. De Andrade, P.C.G.da.S. Vellasco, J.G.S. Da Silva, Sistema construtivo e montagem estrutural do palco principal do Rock in Rio III, Construcao Mag. 7 (2003) 30–35 (in Portuguese).

[35] L.L. Hu, P. Feng, Y.R. Meng, J. Yang, Buckling behavior analysis of prestressed CFRP-reinforced steel columns via FEM and ANN, Eng. Struct. 245 (2021) 112853, http://dx.doi.org/10.1016/j.engstruct.2021.112853.

[36] H. Zhou, V.K.R. Kodur, H. Nie, et al., Behavior of prestressed stayed steel columns under fire conditions, Int. J. Steel Struct. 17 (2017) 195–204, http://dx.doi.org/10.1007/s13296-015-0074-4.

[37] L.L. Hu, E. Ghafoori, S. Pons, P. Feng, J. Yang, I. Azim, Fire behavior and design of steel columns reinforced by prestressed CFRP strips, Compos. Struct. 275 (2021) 114516, http://dx.doi.org/10.1016/j.compstruct.2021.114516.

[38] S. Sánchez-Sáez, T. Gómez-del Rıo, E. Barbero, R. Zaera, C. Navarro, Static behavior of CFRPs at low temperatures, Composites B 33 (2002) 383–390, http://dx.doi.org/10.1016/S1359-8368(02)00021-5.

[39] Y.F. Ou, D.J. Zhu, H.A. Zhang, Y.M. Yao, B. Mobasher, L. Huang, Mechanical properties and failure characteristics of CFRP under intermediate strain rates and varying temperatures, Composites B 95 (2016) 123–136, http://dx.doi.org/10.1016/j.compositesb.2016.03.085.

[40] Q. Cong, Design and Mechanical Properties Characterization of Epoxy Composite Material Used for Cryogenic Field, Harbin Institute of Technology, Harbin, 2016 (in Chinese).

[41] L.L. Hu, M.Y. Li, T. Yiliyaer, W.Y. Gao, H.T. Wang, Strengthening of cracked DH36 steel plates by CFRP sheets under fatigue loading at low temperatures, Ocean Eng. 243 (2022) 110203, http://dx.doi.org/10.1016/j.oceaneng.2021.110203.

[42] EN1993-1-2, Eurocode 3, Design of Steel Structures- Part 1-2: General Rules-Structural Fire Design, CEN, 2005.

[43] R.L. Powell, W.A. Blanpied, Thermal Conductivity of Metals and Alloys At Low Temperatures. A Review of the Literature, National Bureau of Standards Circular, Washington DC, 1954.

[44] Y.N. Tsiovkin, V.D. Sukhanov, Specific heat of some steels and alloys at 10–300 °K, Met. Sci. Heat Treat. 9 (1967) 702–703, http://dx.doi.org/10.1007/BF00649058.

[45] Y.H. Xing, W.Y. Wang, H. Al-azzani, Assessment of thermal properties of various types of high-strength steels at elevated temperatures, Fire Saf. J. 122 (2021) 103348, http://dx.doi.org/10.1016/j.firesaf.2021.103348.

[46] R.J. Corruccini, J.J. Gniewek, Thermal Expansion of Technical Solids at Low Temperatures: A Compilation from the Literature, National Bureau of Standards, Washington DC, 1961.

[47] J.B. Shi, Research on Thermal Expansion Properties of EP and CFRP at Ultra-Low Temperature, Harbin Institute of Technology, 2016 (in Chinese).

[48] Y.J. Chen, X.J. Ren, P. Zhang, T. Zhang, A.B. Wu, Measurement of thermal conductivity of CFRPs and thermal conductance of the cold-to-warm joint at low temperatures, IEEE Trans. Appl. Supercond. 22 (2012) 7700704, https://ieeexplore.ieee.org/document/6086729.

[49] F.S. Makarem, F. Abed, Nonlinear finite element modeling of dynamic localizations in high strength steel columns under impact, Int. J. Impact Eng. 52 (2013) 47–61, http://dx.doi.org/10.1016/j.ijimpeng.2012.10.006.

[50] H. Chen, J.Y. Richard Liew, Explosion and fire analysis of steel frames using mixed element approach, J. Eng. Mech. 131 (6) (2005) 606–616, http://dx.doi.org/10.1061/(ASCE)0733-9399(2005)131:6(606).

[51] H.H. Hafez, M.C. Temple, J.S. Ellis, Pretensioning of single cross arm stayed columns, J. Struct. Div. 105 (2) (1979) 359–375, https://ascelibrary.org/doi/10.1061/JSDEAG.0005098.

[52] L.L. Hu, P. Feng, Theoretical analysis and design of prestressed CFRP-reinforced steel columns, J. Compos. Constr. 26 (3) (2022) 04022029, https://ascelibrary.org/doi/full/10.1061/(ASCE)CC.1943-5614.0001210.